fractal and fractional

MDPI

Article

Influence of the Fractal Distribution of Particle Size on the Critical State Characteristics of Calcareous Sand

Xue Shen [1], Yang Shen [1,*], Junhong Xu [2] and Hanlong Liu [1,3]

[1] Key Laboratory of Ministry of Education for Geomechanics and Embankment Engineering, Hohai University, Nanjing 210024, China; 170804010002@hhu.edu.cn (X.S.); hliu@hhu.edu.cn (H.L.)
[2] School of Civil Engineering, Nanjing Forestry University, Nanjing 210037, China; jhxu@njfu.edu.cn
[3] School of Civil Engineering, Chongqing University, Chongqing 400044, China
* Correspondence: 20070060@hhu.edu.cn

Abstract: To study the influence of the fractal distribution of particle size on the critical state characteristics of calcareous sand, a type of calcareous sand from a certain reef of the South China Sea was used in this study. For comparison, standard quartz sand was also used. A series of drained shear tests on the two sands were then conducted to investigate their critical state characteristics. It was demonstrated that the fractal dimension is suitable for characterizing the particle size distribution (PSD) of calcareous sand with different fine sand content. The critical state equation of sand proposed by Li and Wang (1998) is suitable for fitting the critical state line of calcareous sand. In the plane of deviatoric stress versus the effective confining pressure (q–p' plane) and the plane of void ratio versus $(p'/p_a)^{\alpha}$, the critical state lines of calcareous sand are always above those of quartz sand. The critical state lines of calcareous sand with different fractal dimensions in the q–p' plane are unique. However, in the e–$(p'/p_a)^{\alpha}$ plane, the critical state lines appear to rotate anticlockwise as the fractal dimension increases. In addition, there is an "intersection" in the e–$(p'/p_a)^{\alpha}$ plane. Considering the influence of the fractal distribution of particle size, an expression for the critical state line of calcareous sand in the e–$(p'/p_a)^{\alpha}$ plane was proposed. The related constitutive model was also revised, where a complete set of model parameters suitable for modeling calcareous sand was provided.

Keywords: calcareous sand; fractal dimension; particle size distribution; critical state; shear characteristic

Citation: Shen, X.; Shen, Y.; Xu, J.; Liu, H. Influence of the Fractal Distribution of Particle Size on the Critical State Characteristics of Calcareous Sand. *Fractal Fract.* **2022**, *6*, 165. https://doi.org/10.3390/fractalfract6030165

Academic Editor: Zine El Abiddine Fellah

Received: 16 February 2022
Accepted: 14 March 2022
Published: 17 March 2022

1. Introduction

As the main foundation material for construction in the South China Sea, calcareous sand is a type of marine biogenic sand. Its chemical composition is different from that of common terrestrial sand and marine sand; the calcium carbonate content is more than 50%. It is characterized by an extremely irregular particle shape, high friction angle, high porosity (including internal porosity), high compressibility, brittleness of grains, and so on [1–10]. The calcareous sand from the South China Sea is composed of coral debris, and the calcium carbonate content is mostly above 90% [4]. These characteristics make its basic mechanical properties more complicated than those of quartz sand [11–13]. It is of great significance to study its mechanical properties. Recent research on the calcareous sand in the South China Sea found that its particle breakage is far less than that in previous research under the same load condition [14]. This may be related to its generation environment, hydraulic fill method, and so on [5,15]. Compared with the original calcareous sand, the dredger fill calcareous sand is not easily broken because of the breakage during hydraulic fill. In addition, the confining pressure plays an important role in the drained shear properties of calcareous sand [16–18]. Compared with quartz sand, the volumetric deformation, internal friction angle, and shear strength of calcareous sand are larger [19–21].

The critical state refers to the state in which the axial deformation of soil develops continuously without volumetric change under constant stress [22]. It is often used to

design and evaluate the long-term strength of buildings (structures) in engineering practice. The design of filled islands also relies on the concept of critical state strength [23,24]. Early studies based on clay assumed that the critical state line is a straight line in the plane of void ratio versus the logarithm of the effective confining pressure (e–lgp' plane) [22]. However, for granular materials, it has been found that the critical state line is not a straight line. Thus, a series of critical state equations have been introduced [25–27]. Li and Wang [28] suggested that the critical state line of sandy soil is approximately a straight line in the e–$(p'/p_a)^{\alpha}$ plane based on the data from previous research. Based on this, the critical state line of quartz sand can be well fit within the stress range of 10~500 kPa. This conclusion is widely used [29]. However, calcareous sand is multangular and irregular, leading to more complicated mechanical properties compared to quartz sand. It remains to be studied whether the existing critical state theory is suitable for calcareous sand.

Recently, fractal theory has been widely used in respectively describing and studying the particle size distribution, the pore size distribution, the particle morphology, and so on [30–35]. The particle size distribution (PSD) has a significant impact on the critical state characteristics of sand [36,37]. Particle breakage can lead to a sharp increase in fine sand content. Moreover, seepage can lead to a significant decrease in fine sand content. Both of these two conditions will significantly change the fine sand content of calcareous sand. Then, the critical state characteristics of calcareous sand are affected. Therefore, it is necessary to study the effect of fine sand content on the triaxial shear and critical state characteristics of calcareous sand. However, the effect of the fractal distribution of particle size on the critical state characteristics of calcareous sand is still poorly understood.

To reveal the particularity of calcareous sand, quartz sand was used as a reference for comparison in this study. Triaxial tests of the two sands were performed to investigate their critical state characteristics. The applicability of the critical state theory to calcareous sand was analyzed. The influence of the fractal distribution of particle size on the critical state characteristics of calcareous sand was studied. The relationship between the fractal dimension and the critical state characteristics of calcareous sand was established. Based on this, the related constitutive model was revised. A complete set of model parameters suitable for calcareous sand was given.

2. Materials and Methods

The calcareous sand used in this study was from a certain reef of the South China Sea. The influence of the content of particles smaller than 0.25 mm ($P_{0.25}$) is researched in this paper. When $P_{0.25}$ is changed, the relative content of the rest of the particle fractions remains the same. According to this method, the designed gradation is similar to the actual gradation. Table 1 shows the test grain size distribution of the calcareous sand and quartz sand. The gradation in bold is the actual gradation. The gradation curves of the calcareous sand with different $P_{0.25}$ are shown in Figure 1.

Table 1. Test grain size distribution of the calcareous sand and quartz sand.

Particle Fraction (mm)	5~2	2~1	1~0.5	0.5~0.25	0.25~0.075	<0.075
Calcareous sand	9.9%	7.3%	33.5%	34.3%	14.2%	0.8%
	8.8%	6.5%	29.5%	30.2%	23.7%	1.3%
	7.6%	**5.6%**	**25.6%**	**26.2%**	**33.1%**	**1.9%**
	6.4%	4.7%	21.7%	22.2%	42.6%	2.4%
	5.3%	3.9%	17.7%	18.1%	52.1%	2.9%
Quartz sand	7.6%	5.6%	25.6%	26.2%	33.1%	1.9%

To study the specific calcareous sand, quartz sand was adopted as a reference for comparison. Table 2 shows the basic property parameters of the calcareous sand and quartz sand with the same gradation ($P_{0.25}$ = 35%).

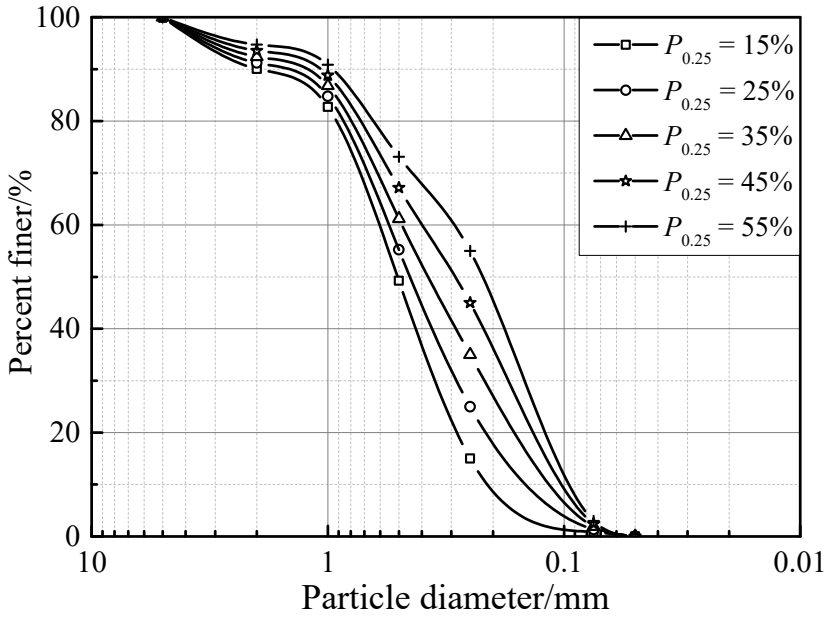

Figure 1. Grain size distribution curve of the tested calcareous sand.

Table 2. Basic property parameters of the test sands ($P_{0.25}$ = 35%).

Sample	Coefficient of Uniformity (C_u)	Coefficient of Curvature (C_c)	Maximum Void Ratio (e_{max})	Minimum Void Ratio (e_{min})	Specific Gravity (*Gs*)
Calcareous sand	4.8	0.9	1.19	0.80	2.70
Quartz sand	4.8	0.9	0.75	0.39	2.67

Figure 2 presents the 3-D morphology characteristics of the tested calcareous sand and quartz sand particles according to the CT scanner. It can be seen that, compared with quartz sand, the particles of calcareous sand are multiangular, flatter, and more irregular. The calcareous sand particles have more internal pores and their surface is uneven. When the calcareous sand is compressed with a vertical load of 4000 kPa, the relative breakage B_r [38] is only 0.7% (0~1) [39]. This shows that the particle breakage of this type of calcareous sand is insignificant and can be ignored. This conclusion is similar to that of the aforementioned research [14]. Therefore, this paper focuses on exploring the influence of the fractal distribution of particle size on the critical state characteristics of calcareous sand, without considering the impact of particle breakage.

A strain path triaxial apparatus was used to conduct a series of drained shear tests (CD tests). The shear characteristics of the calcareous sand with different fractal distributions of particle size were studied. The diameter and height of the test samples were 61.8 and 135 mm, respectively. The calcareous sand used in the test was saturated by applying head pressure and back pressure. When the B-value (i.e., saturation) [40] was greater than 0.98, the sample was considered saturated. Four effective confining pressures (100, 200, 300, and 400 kPa) were conducted. The tests were conducted using a constant vertical shear rate of 0.016mm/min until the axial strain achieved 25%. It should be noted that the average value of the critical state data in the last 3% strain range was used as the final value.

Four drained shear tests for quartz sand ($P_{0.25}$ = 35%) with different effective confining pressures were conducted as comparisons. The relative densities of the sand samples were all 40%.

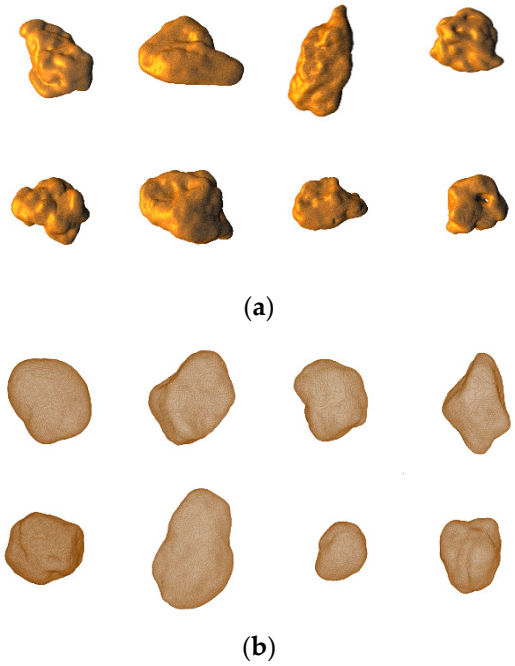

(**a**)

(**b**)

Figure 2. CT scan images of the tested calcareous sand and quartz sand particles: (**a**) calcareous sand particles; (**b**) quartz sand particles.

3. Experiments

3.1. Fractal Behavior of Particle Size Distribution

Recently, fractal theory has been widely used in respectively describing and studying the geometric features of the PSD. Tyler et al. [41] proposed the fractal model of particle size distribution. It was expressed with the relationship between the cumulative mass and particle size of the particles, as follows:

$$\frac{M(\delta < d_i)}{M_t} = \left(\frac{d_i}{d_{\max}}\right)^{3-D_{\mathrm{m}}} \tag{1}$$

The fractal dimension D_{m} can be determined by:

$$\lg\left(\frac{M(\delta < d_i)}{M_t}\right) = (3 - D_{\mathrm{m}})\lg(d_i) + (D_{\mathrm{m}} - 3)\lg(d_{\max}) \tag{2}$$

where δ is the particle size, d_i is the diameter of the ith (i = 1, 2, . . . , n) sieve pore, $M(\delta < d_i)$ is the cumulative mass of the sand particles whose grain size is smaller than d_i, M_t is the total mass of sand particles, $d_{\max}$ is the maximum grain size, and D_{m} is the fractal dimension.

However, only one fractal dimension is not enough to describe the distribution for the entire range of particle sizes [42,43]. Posadas et al. [42] applied multifractal techniques to describe contrasting PSDs. The dominant particles of calcareous sand are distributed in the large size range (i.e., the particle size greater than 0.075 mm). As shown in Figure 3, the fractal dimension of the PSD (i.e., the particle size greater than 0.075 mm) was obtained through the regression analysis based on Equation (2). The fitting results of fractal dimensions reveal that the particle size distribution of calcareous sand complies with the fractal law.

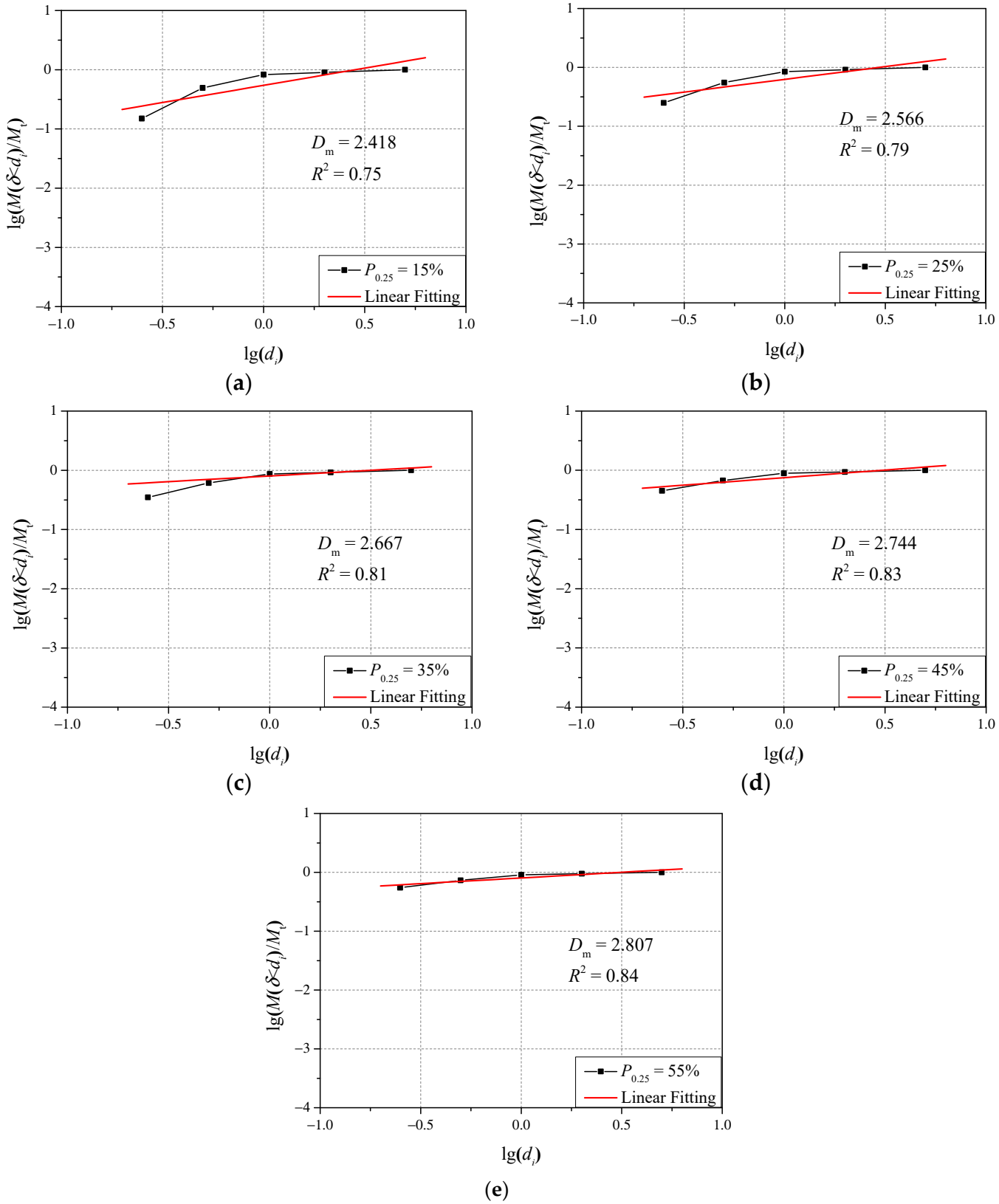

Figure 3. Determination of fractal dimensions of calcareous sand with different gradation: (**a**) content of particles smaller than 0.25 mm is 15%; (**b**) content of particles smaller than 0.25 mm is 25%; (**c**) content of particles smaller than 0.25 mm is 35%; (**d**) content of particles smaller than 0.25 mm is 45%; (**e**) content of particles smaller than 0.25 mm is 55%.

Figure 4 shows the fractal dimensions of the tested calcareous sand with different gradation. As is shown, the higher the content of fine materials in the PSD is, the larger the value of D_m is. The relationship between the $P_{0.25}$ and D_m is almost linear (R^2 = 0.96). Therefore, the fractal dimension can be well used to characterize the gradation of the calcareous sand with different fine sand content.

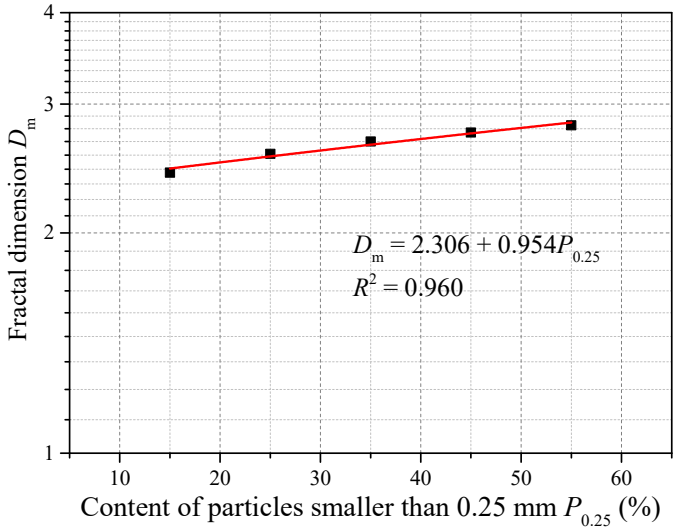

Figure 4. Fractal dimensions of the calcareous sand with different gradation.

3.2. Critical State Characteristics of the Calcareous Sand

Figure 5 shows the critical state lines in the plane of deviatoric stress versus the effective confining pressure (q–p' plane) of the calcareous sand and quartz sand (D_m = 2.667).

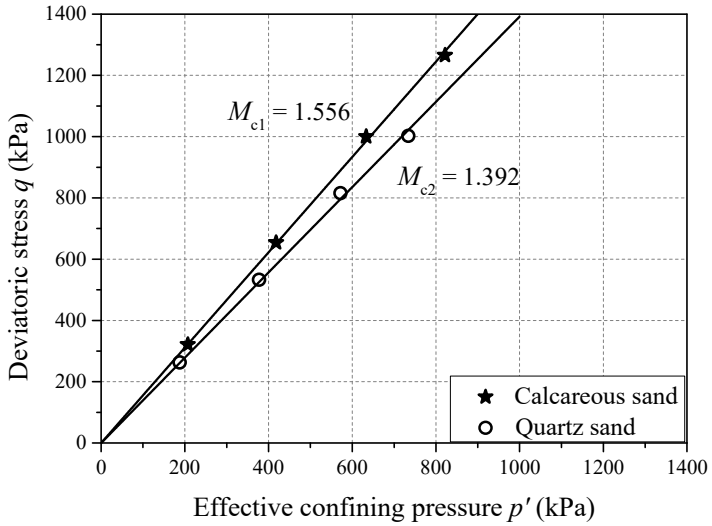

Figure 5. The critical state lines in the q–p' plane of the calcareous sand and quartz sand (D_m = 2.667).

As is shown, the critical stress ratio of calcareous sand (M_{c1} = 1.556) is approximately 12% higher than that of quartz sand (M_{c2} = 1.392). The critical stress ratio reflects the particle interlocking. Its value depends primarily on the particle mineralogy and shape (angularity) [44]. The particles of calcareous sand are more angular than those of quartz sand, leading to stronger particle interlocking. As the damaged calcareous sand reached the critical state, q reached a constant value. The initial sand fabric was destroyed at this condition. The residual strength of calcareous sand is larger due to the stronger particle interlocking.

The sand critical state equation put forward by Li and Wang [28] is used to fit the critical state line of calcareous sand in the e–p' plane, as shown in the following Equation (3):

$$e_c = e_{c0} - \lambda \left(\frac{p'}{p_a}\right)^{\alpha} \tag{3}$$

where e_c is the critical void ratio; e_{c0}, λ, and α are the material constants determining the critical state line in the e–p' plane [28], and p_a is the atmospheric pressure for normalization. α is a material parameter affected by the material type and the modulus type. The effect of the value of α on the straightness of the lines is mild; α can be simply chosen as a default value [28]. For the calcareous sand analyzed in this article, α can be taken as 0.55. For the quartz sand analyzed in this article, α can be taken as 0.71. Based on this, the critical state lines in the e–$(p'/p_a)^{\alpha}$ plane of the calcareous sand and quartz sand (D_m = 2.667) are as shown in Figure 6.

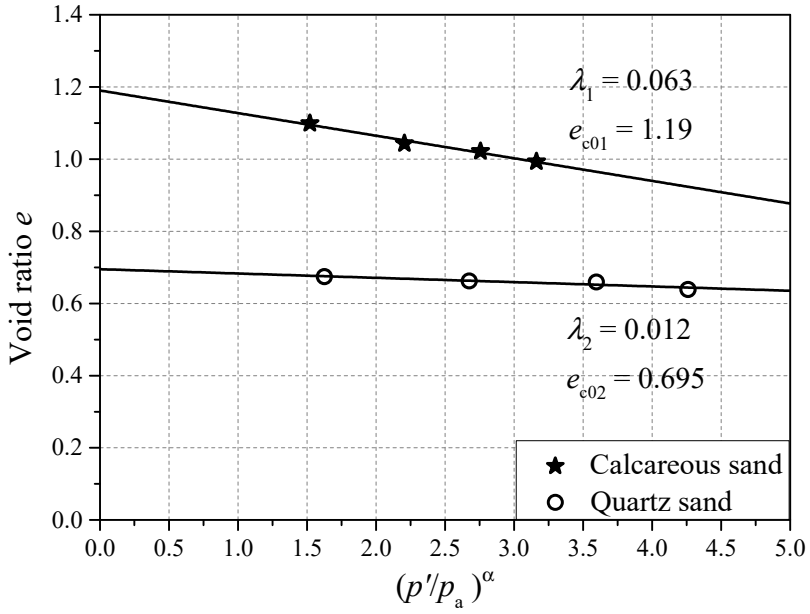

Figure 6. The critical state lines in the e–$(p'/p_a)^{\alpha}$ plane of the calcareous sand and quartz sand (D_m = 2.667).

As is shown in Figure 6, the critical state lines of the calcareous sand and quartz sand can be plotted as nearly straight in the e versus $(p'/p_a)^{\alpha}$ plane proposed by Li and Wang [28]. The critical state line of calcareous sand is always above that of quartz sand with the same gradation. The critical state parameter λ and e_{c0} values of the calcareous sand are all larger than those of the quartz sand. The higher initial void ratio of the calcareous sand results in a larger e_{c0}. Moreover, the larger slope λ indicates the greater influence of confining pressure on the critical state void ratio of calcareous sand [39].

3.3. Influence of the Fractal Distribution of Particle Size on the Critical State Line in the q–p' Plane of the Calcareous Sand

Figure 7 shows the critical state line in the q–p' plane of the calcareous sand with different fractal dimensions.

As is shown, the critical state points of calcareous sand with different fractal dimensions basically fall along the same critical state line (M_c = 1.575) in the q–p' plane (R^2 = 92.61%). Therefore, the critical state lines of calcareous sand with different fractal dimensions in the q–p' plane are unique. The critical stress ratio M_c of the calcareous sand with different fractal dimensions is a constant. This conclusion is the same as those of other sands in related research [45,46].

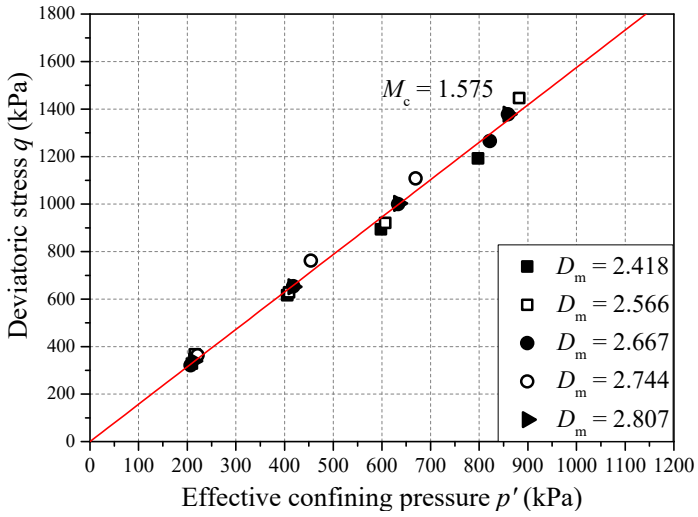

Figure 7. The critical state line in the q–p' plane of the calcareous sand with different fractal dimensions.

3.4. Influence of the Fractal Distribution of Particle Size on the Critical State Line in the e–p′ Plane of the Calcareous Sand

The critical state lines in the e–$(p'/p_a)^{\alpha}$ plane of the calcareous sand with different fractal dimensions are shown in Figure 8.

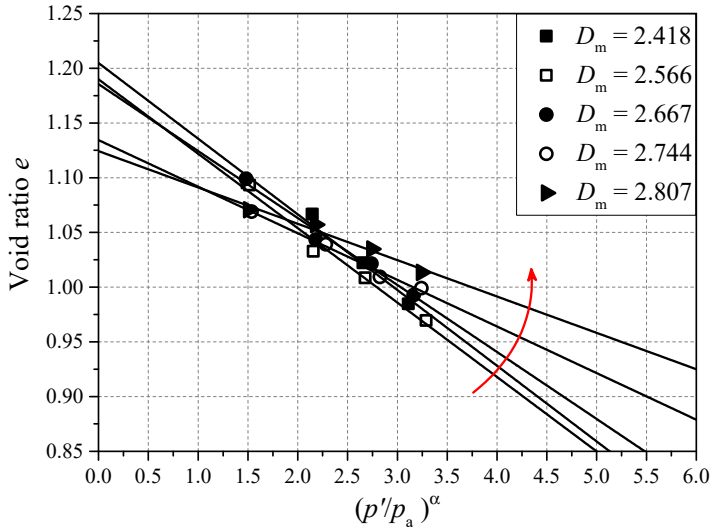

Figure 8. The critical state lines in the e–$(p'/p_a)^{\alpha}$ plane of the calcareous sand with different fractal dimensions.

It can be found that with the increase in fractal dimension, the critical state parameter λ and e_{c0} of calcareous sand both decrease. The same is true for the Hoston sand. However, the slope λ of the critical state lines of the calcareous sand changes more significantly than that of the Hoston sand [36].

With the increase in fractal dimension, the fine sand content of calcareous sand increases. The pores formed by the coarse particles are filled by the fine particles. The initial void ratio of the calcareous sand decreases and the critical state parameter e_{c0} decreases. The smaller initial void ratio leads to a weaker influence of confining pressure on the critical state void ratio of calcareous sand, and the slope λ of the critical state line of the calcareous sand decreases.

Figure 8 also shows that the critical state lines in the e–$(p'/p_a)^{\alpha}$ plane appear to rotate anticlockwise approximately as the fractal dimension increases. When $(p'/p_a)^{\alpha}$ is equal to 2.2, the critical state void ratios of calcareous sand with different fractal dimensions are

around 1.05. This means that there is an "intersection" in the e–$(p'/p_a)^{\alpha}$ plane. When the effective confining pressure p' is equal to 425 kPa, the critical void ratios of the calcareous sand with different fractal dimensions are approximately the same.

Based on this, the critical state of calcareous sand in the e–$(p'/p_a)^{\alpha}$ plane can be expressed as:

$$e_c - b = -\lambda\left[\left(\frac{p\prime}{p_a}\right)^{\alpha} - a\right] \tag{4}$$

$$e_c = b + a\lambda - \lambda\left(\frac{p\prime}{p_a}\right)^{\alpha} \tag{5}$$

where a and b are material constants. They are also the "intersection point" coordinates of the critical state lines in the e–$(p'/p_a)^{\alpha}$ plane.

By combining Equations (3) and (5), the parameter e_{c0} can be written as:

$$e_{c0} = b + a\lambda \tag{6}$$

Figure 9 shows the relationship between the reference void ratio e_{c0} and slope of critical state lines λ.

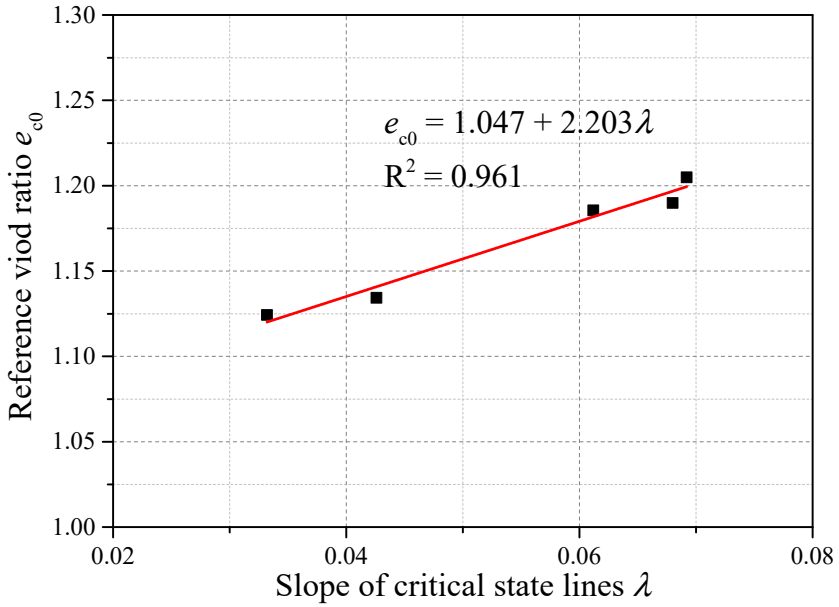

Figure 9. Relationship between reference void ratio e_{c0} and slope of critical state lines λ.

As is shown in Figure 9, there is indeed a linear relationship between the reference void ratio e_{c0} and slope of critical state lines λ (R^2 = 0.961). For the calcareous sand analyzed in this article, a is 2.203 and b is 1.047.

Figure 10 presents the relationship between the slope of critical state lines λ and fractal dimension D_{m}.

Second-order functions can be applied to fit the relationship, as follows:

$$\lambda = cD_{\mathrm{m}}{}^2 + dD_{\mathrm{m}} + f \tag{7}$$

where c, d, and f are material constants. For the calcareous sand analyzed in this paper, c is -0.384, d is 1.908, and f is -2.302.

Figure 11 shows the comparison of material constants determined by the model with experimental data.

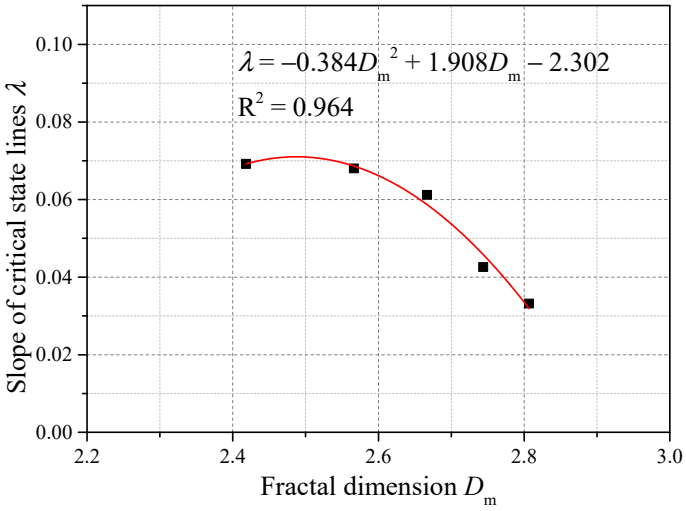

Figure 10. Relationship between slope of critical state lines λ and fractal dimension D_m.

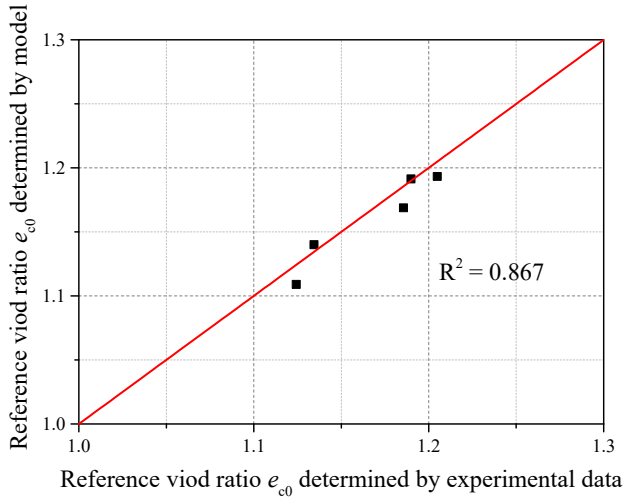

(**a**)

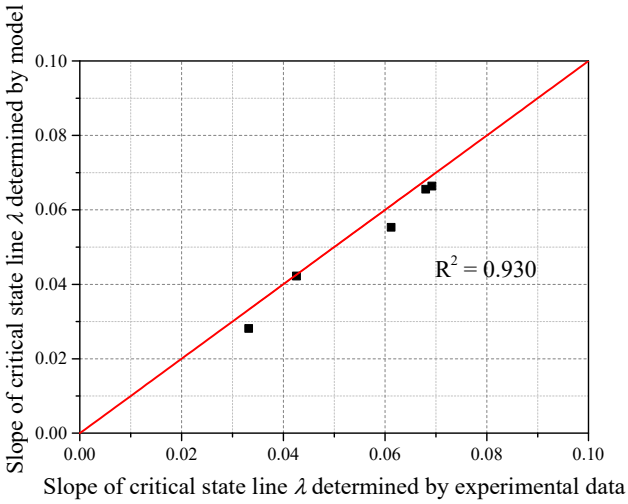

(**b**)

Figure 11. Comparison of material constants determined by the model with experimental data: (**a**) reference void ratio e_{c0}; (**b**) slope of critical state lines λ.

As can be seen, the material constants determined by the model and those determined by the experimental data are highly correlated. The model expressed as Equations (4)–(7) can be used to predict the material parameters of calcareous sand with different fractal dimensions.

By combining Equations (5) and (7), considering the influence of the fractal distribution of particle size, an expression for the critical state of calcareous sand in the e–$(p'/p_a)^{\alpha}$ plane is proposed:

$$e_c = b + a\left(cD_m{}^2 + dD_m + f\right) - \left(cD_m{}^2 + dD_m + f\right)\left(\frac{p\prime}{p_a}\right)^{\alpha} \tag{8}$$

4. Theoretical Model

The expression of state-dependent dilatancy put forward by Li et al. [47] was used in this paper, as follows:

$$d = d_0\left(e^{m\psi} - \frac{\eta}{M}\right) \tag{9}$$

where d_0 and m are two modeling parameters, η is the stress ratio, and Ψ is a state parameter. Ψ is defined as:

$$\psi = e - e_c \tag{10}$$

Considering the influence of the fractal distribution of particle size, e_c can be expressed by Equation (8). The state parameter Ψ is proposed:

$$\psi = e - b - a\left(cD_m{}^2 + dD_m + f\right) + \left(cD_m{}^2 + dD_m + f\right)\left(\frac{p\prime}{p_a}\right)^{\alpha} \tag{11}$$

The state-dependent constitutive model established by Li et al. [47] was used in this paper, as follows:

$$\left\{ \begin{array}{c} dq \\ dp\prime \end{array} \right\} = \left[\left(\begin{array}{cc} 3G & 0 \\ 0 & K \end{array} \right) - \frac{h(L)}{K_p + 3G - K\eta d} \left(\begin{array}{cc} 9G^2 & -3KG\eta \\ 3KGd & -K^2\eta d \end{array} \right) \right] \left(\begin{array}{c} d\varepsilon_q \\ d\varepsilon_v \end{array} \right) \tag{12}$$

where G is the elastic shear modulus, K is the elastic bulk modulus, L is a loading index, K_p is the plastic modulus, and $h(L)$ is a Heaviside function with $h(L) = 1$ for $L > 0$ and $h(L) = 0$ otherwise.

The elastic shear modulus G can be calculated by the following empirical equation [48]:

$$G = G_0 \frac{(2.97 - e)^2}{1 + e} \sqrt{p\prime p_a} \tag{13}$$

where G_0 is a material constant, and e_{c0} is the initial void ratio. The elastic bulk modulus K can be calculated based on elasticity theory, as follows:

$$K = G \frac{2(1 + v)}{3(1 - 2v)} \tag{14}$$

where ν is the Poisson's ratio.

The constitutive relation is put forward to express the plastic modulus K_p:

$$K_p = hG\left(\frac{M}{\eta} - e^{n\psi}\right) \tag{15}$$

$$h = h_1 - h_2 e \tag{16}$$

where h_1, h_2, and n are three material constants.

5. Model Validation

Figure 12 presents the relationship between the phase transformation state stress ratio and peak state stress ratio and the state parameter of calcareous sand. As is shown, as the ψ increases, the M_d increases and the M_p decreases. Equations proposed by Li and Dafalias [47] are used to quantify such evolutions, as follows:

$$M_d = A_d M_c \exp(m\psi) \tag{17}$$

$$M_p = A_p M_c \exp(-n\psi) \tag{18}$$

where A_d and A_p are the correction factor. m and n are material constants. For the calcareous sand analyzed in this article, m is 0.7438 and n is 0.5698.

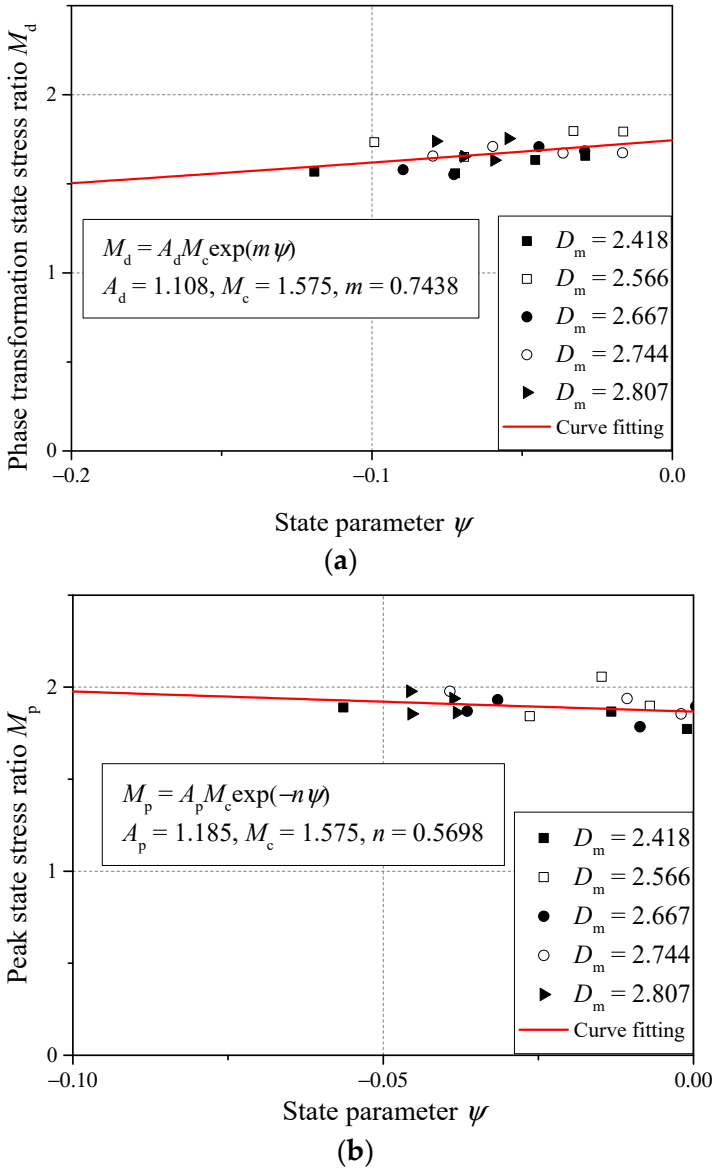

Figure 12. Relationship between state stress ratio and state parameter: (**a**) phase transformation state stress ratio; (**b**) peak state stress ratio.

As shown in Table 3, fourteen material constants are used in the model. All these parameters can be calibrated by a systematic procedure based on triaxial data.

Table 3. Model parameters calibrated for calcareous sand.

Elastic Parameters	Critical State Parameters		Dilatancy Parameters	Hardening Parameters
G_0 =125	M = 1.58	d = 1.91	d_0 = 6.05	h_1 = 3.35
ν = 0.30	a = 2.20	f = −2.30	m = 0.74	h_2 = 3.05
	b = 1.05	α = 0.55		n = 0.57
	c = −0.38			

6. Conclusions

To study the effect of the fractal distribution of particle size on the critical state characteristics of calcareous sand, a type of calcareous sand from the South China Sea was adopted in this study. For comparison, standard quartz sand was also used. A series of drained shear tests on the two sands were performed to research their critical state characteristics. Conclusions were drawn as follows:

(1) The particle size distribution of calcareous sand can obey the fractal law. The higher the fine sand content in the PSD was, the larger the value of D_{m} was. The fractal dimension can be used to characterize the particle size distribution of calcareous sand with different fine sand content.

(2) The critical stress ratio of calcareous sand (M_c = 1.556) was around 12% higher than that of quartz sand (M_c = 1.392), and its critical state line parameters λ and e_{c0} were also larger than those of quartz sand. In the q–p' plane and e–$(p'/p_a)^{\alpha}$ plane, the critical state lines of calcareous sand were always above those of the quartz sand.

(3) The critical state lines of calcareous sand with different fractal dimensions in the q–p' plane were unique.

(4) The critical state equation of sand proposed by Li and Wang [28] was suitable for the fitting of the critical state line of calcareous sand in the e–$(p'/p_a)^{\alpha}$ plane.

(5) In the e–$(p'/p_a)^{\alpha}$ plane, the critical state lines appeared to rotate anticlockwise as the fractal dimension increased. There was an "intersection" in the e–$(p'/p_a)^{\alpha}$ plane. When the effective confining pressure p' was equal to 425 kPa, the critical void ratios of the calcareous sand with different fractal dimensions were approximately the same. Considering the influence of the fractal distribution of particle size, an expression for the critical state of calcareous sand in the e–$(p'/p_a)^{\alpha}$ plane was proposed.

(6) Based on the critical state characteristics of calcareous sand with different fractal dimensions, the dilatancy equation and constitutive model suitable for calcareous sand were proposed. Moreover, a complete set of model parameters suitable for calcareous sand was given.

Author Contributions: Conceptualization, Y.S. and H.L.; methodology, X.S. and Y.S.; formal analysis, X.S. and J.X.; investigation, X.S. and J.X.; resources, Y.S. and H.L.; writing—original draft preparation, X.S. and Y.S.; funding acquisition, Y.S. and X.S. All authors have read and agreed to the published version of the manuscript.

Funding: This work was financially supported by the National Natural Science Foundation of China (No. 51979087), the Postgraduate Research and Practice Innovation Program of Jiangsu Province (KYCX20_0435), the Fundamental Research Funds for the Central Universities (No. B200203080), and the China Scholarship Council (No. 202006710143).

Institutional Review Board Statement: Not applicable.

Informed Consent Statement: Not applicable.

Data Availability Statement: Not applicable.

Acknowledgments: The authors would like to thank Yifei Sun from Ruhr-University Bochum for his kind suggestions and help.

Conflicts of Interest: The authors declare no conflict of interest.

References

1. Coop, M.R. The mechanics of uncemented carbonate sands. *Géotechnique* **1990**, *40*, 607–626. [CrossRef]
2. Datta, M.; Gulhati, S.K.; Rao, G.V. Crushing of calcareous sands during drained shear. *Soc. Pet. Eng. J.* **1980**, *20*, 77–85. [CrossRef]
3. Yasser, D.; Habib, S.; Hossein, S.; Reza, R. Compressibility and undrained behavior of hormuz calcareous sand. *Electron. J. Geotech. Eng.* **2010**, *15*, 1684–1702.
4. Liu, C.Q.; Yang, Z.Q.; Wang, R. Preliminary research on physical and mechanical properties of calcareous sand. *Rock Soil Mech.* **1998**, *19*, 32–37.
5. Shahnazari, H.; Rezvani, R. Effective parameters for the particle breakage of calcareous sands: An experimental study. *Eng. Geol.* **2013**, *159*, 98–105. [CrossRef]
6. Wang, G.; Wang, Z.; Ye, Q.; Zha, J. Particle breakage evolution of coral sand using triaxial compression tests. *J. Rock Mech. Geotech. Eng.* **2021**, *13*, 321–334. [CrossRef]
7. Cao, Z.; Chen, J.; Ye, X.; Gu, C.; Guo, Z.; Cai, Y. Experimental study on particle breakage of carbonate gravels under cyclic loadings through large-scale triaxial tests. *Transp. Geotech.* **2021**, *30*, 100632. [CrossRef]
8. Xiao, Y.; Yuan, Z.; Chu, J.; Liu, H.L.; Huang, J.; Luo, S.N.; Wang, S.; Lin, J. Particle breakage and energy dissipation of carbonate sands under quasi-static and dynamic compression. *Acta Geotech.* **2019**, *14*, 1741–1755. [CrossRef]
9. Altuhafi, F.; O'Sullivan, C.; Cavarretta, I. Analysis of an image-based method to quantify the size and shape of sand particles. *J. Geotech. Geoenviron. Eng.* **2013**, *139*, 1290–1307. [CrossRef]
10. Wang, X.Z.; Jiao, Y.Y.; Wang, R.; Hu, M.J.; Meng, Q.S.; Tan, F.Y. Engineering characteristics of the calcareous sand in Nansha Islands, South China Sea. *Eng. Geol.* **2011**, *120*, 40–47. [CrossRef]
11. Cui, M.J.; Zheng, J.J.; Chu, J.; Wu, C.C.; Lai, H.J. Bio-mediated calcium carbonate precipitation and its effect on the shear behaviour of calcareous sand. *Acta Geotech.* **2021**, *16*, 1377–1389. [CrossRef]
12. Hasanlourad, M.; Salehzadeh, H.; Shahnazari, H. Dilation and particle breakage effects on the shear strength of calcareous sands based on energy aspects. *Int. J. Civ. Eng.* **2008**, *6*, 108–119.
13. Li, Y.; Lin, Z.; Li, B.; He, L.; Gong, J. Effects of gradation and grain crushing on the liquefaction resistance of calcareous sand. *Geomech. Geophys. Geo-Energy Geo-Resour.* **2021**, *7*, 12. [CrossRef]
14. Wang, Y.Q.; Hong, Y.; Guo, Z.; Wang, L.Z. Micro- and macro-mechanical behavior of crushable calcareous sand in South China Sea. *Rock Soil Mech.* **2018**, *39*, 199–206.
15. Qin, Y.; Yao, T.; Wang, R.; Zhu, C.Q.; Meng, Q.S. Particle breakage-asad analysis of deformation law of calcareous sediments under high-pressure consolidation. *Rock Soil Mech.* **2014**, *35*, 3123–3128.
16. Lagioia, R.; Nova, R. An experimental and theoretical study of the behaviour of a calcarenite in triaxial compression. *Géotechnique* **1995**, *45*, 633–648. [CrossRef]
17. Sharma, S.S.; Fahey, M. Degradation of Stiffness of Cemented Calcareous Soil in Cyclic Triaxial Tests. *J. Geotech. Geoenviron.* **2003**, *129*, 619–629. [CrossRef]
18. Sharma, S.S.; Fahey, M. Deformation characteristics of two cemented calcareous soils. *Can. Geotech. J.* **2004**, *41*, 1139–1151. [CrossRef]
19. Zhang, J.M.; Jiang, G.S.; Wang, R. Research on influences of particle breakage and dilatancy on shear strength of calcareous sands. *Rock Soil Mech.* **2009**, *30*, 2043–2048.
20. He, S.H.; Shan, H.F.; Xia, T.D.; Liu, Z.J.; Ding, Z.; Xia, F. The effect of temperature on the drained shear behavior of calcareous sand. *Acta Geotech.* **2021**, *16*, 613–633. [CrossRef]
21. He, S.H.; Zhang, Q.; Ding, Z.; Xia, T.D.; Gan, X. Experimental and Estimation Studies of Resilient Modulus of Marine Coral Sand under Cyclic Loading. *J. Mar. Sci. Eng* **2020**, *8*, 287. [CrossRef]
22. Schofield, A.N.; Wroth, P. *Critical State Soil Mechanics*; McGraw-Hill: London, UK, 1968.
23. Sladen, J.A.; D'Hollander, R.D.; Krahn, J.; Mitchell, D.E. Back analysis of the Nerlerk berm liquefaction slides. *Can. Geotech. J.* **1985**, *22*, 579–588. [CrossRef]
24. Cai, Z.Y.; Hou, H.Y.; Zhang, J.X.; Zhang, L.; Guan, Y.F.; Cao, Y.Y. Critical state and constitutive model for coral sand considering particle breakage. *Chin. J. Geotech. Eng.* **2019**, *41*, 7.
25. Riemer, M.F.; Seed, R.B. Factors affecting apparent position of steady-state line. *J. Geotech. Geoenviron.* **1997**, *123*, 281–288. [CrossRef]
26. Manzari, M.; Dafalias, Y. A critical state two-surface plasticity model for sands. *Géotechnique* **1997**, *47*, 255–272. [CrossRef]
27. Maeda, K.; Muir Wood, D.; Nukudani, E. Modelling mechanical consequences of erosion. *Géotechnique* **2010**, *60*, 447–457.
28. Li, X.S.; Wang, Y. Linear Representation of Steady-State Line for Sand. *J. Geotech. Geoenviron.* **1998**, *124*, 1215–1217. [CrossRef]
29. Sun, Y.F.; Wichtmann, T.; Sumelka, W.; Kan, M.E. Karlsruhe fine sand under monotonic and cyclic loads: Modelling and validation. *Soil Dyn. Earthq. Eng.* **2020**, *133*, 106119. [CrossRef]
30. Turcotte, D.L. Fractals and fragmentation. *J. Geophys. Res.* **1986**, *91*, 1921–1926. [CrossRef]

31. Zhang, X.; Hu, W.; Scaringi, G.; Baudet, B.A.; Han, W. Particle shape factors and fractal dimension after large shear strains in carbonate sand. *Geotech. Lett.* **2018**, *8*, 73–79. [CrossRef]
32. Sun, Y.F.; Liu, H.L.; Yang, G. Yielding function for coarse aggregates considering gradation evolution induced by particle breakage. *Rock Soil Mech.* **2013**, *34*, 3479–3484.
33. Li, Y.; Zhang, H.; Huang, M.H.; Yin, H.B.; Jiang, K.; Xiao, K.T.; Tang, S.W. Influence of Different Alkali Sulfates on the Shrinkage, Hydration, Pore Structure, Fractal Dimension and Microstructure of Low-Heat Portland Cement, Medium-Heat Portland Cement and Ordinary Portland Cement. *Fractal Fract.* **2021**, *5*, 79. [CrossRef]
34. He, S.H.; Ding, Z.; Hu, H.B.; Gao, M. Effect of Grain Size on Microscopic Pore Structure and Fractal Characteristics of Carbonate-Based Sand and Silicate-Based Sand. *Fractal Fract.* **2021**, *5*, 152. [CrossRef]
35. Ioelovich, M. Study of Fractal Dimensions of Microcrystalline Cellulose Obtained by the Spray-Drying Method. *Fractal Fract.* **2019**, *3*, 3. [CrossRef]
36. Li, G.; Liu, Y.J.; Yin, Z.Y.; Dano, C.; Hicher, P.Y. Grading effect on critical state behavior of granular materials. *Chin. J. Geotech. Eng.* **2014**, *36*, 452–457.
37. Liu, Y.J.; Wang, J.H.; Yin, Z.Y.; Li, G.; Xia, X.H. Constitutive modeling for granular materials considering grading effect. *Chin. J. Geotech. Eng.* **2015**, *37*, 299–305.
38. Hardin, B.O. Crushing of Soil Particles. *Int. J. Geotech. Eng.* **1985**, *111*, 1177–1192. [CrossRef]
39. Shen, Y.; Shen, X.; Liu, H.L.; Ge, H.Y.; Rui, X.X. Gradation affects basic mechanical characteristics of Chinese calcareous sand as airport subgrade of reefs. *Mar. Georesour. Geotechnol.* **2020**, *38*, 706–715.
40. Skempton, A.W. The pore-pressure coefficients A and B. *Géotechnique* **1954**, *4*, 143–147. [CrossRef]
41. Tyler, S.W.; Wheatacraft, S.W. Fractal scaling of soil particle-size distributions: Analysis and limitations. *Soil Sci. Soc. Am. J.* **1992**, *56*, 362–369. [CrossRef]
42. Posadas, A.N.D.; Giménez, D.; Bittelli, M.; Vaz, C.M.P.; Flury, M. Multifractal characterization of soil particle-size distributions. *Soil Sci. Soc. Am. J.* **2001**, *65*, 1361–1367. [CrossRef]
43. Wang, J.; Cao, L.; Wang, B.; Gong, H.T.; Tang, W. Overview of One-Dimensional Continuous Functions with Fractional Integral and Applications in Reinforcement Learning. *Fractal Fract.* **2022**, *6*, 69.
44. Sadrekarimi, A.; Olson, S. Critical state friction angle of sands. *Géotechnique* **2011**, *61*, 771–783. [CrossRef]
45. Bandini, V.; Coop, M. The influence of particle breakage on the location of the critical state line of sands. *Soil Found.* **2011**, *51*, 591–600. [CrossRef]
46. Luzzani, L.; Coop, M.R. On the relationship between particle breakage and the critical state of sands. *Soil Found.* **2002**, *42*, 71–82. [CrossRef]
47. Li, X.S.; Dafalias, Y.F. Dilatancy for cohesionless soils. *Géotechnique* **2000**, *50*, 449–460. [CrossRef]
48. Richart, F.E.; Hall, J.R.; Woods, R.D. Vibrations of soils and foundations. *Princ. Neurodyn. Spartan* **1970**, *209*, 137.